Direct measurement of yield stress of discrete materials

S. H. Ebrahimnazhad Rahbari [†‡], J. Vollmer [†], S. Herminghaus [†], M. Brinkmann [†]
[†] *Max-Planck Institute for Dynamics and Self-Organization, Department of Complex Fluids, 37073 Göttingen, Germany.*
[‡] *Plasma and condensed matter computational lab, Department of Physics, Faculty of Science, Azarbayjan University of Tarbiat Moallem, Tabriz 53714-161, Iran.**

(Dated: October 24, 2018)

We present a novel computational method for direct measurement of yield stress of discrete materials. The method is well-suited for the measurement of jamming phase diagram of a wide range of discrete particle systems such as granular materials, foams, and colloids. We further successfully apply the method to evaluate the jamming phase diagram of wet granular material in order to demonstrates the applicability of the model.

PACS numbers: 45.70.-n, 62.20.M-, 45.05.+x 45.70.Mg
Keywords: jamming phase diagram, cohesive granular flow, yield stress, failure criterion, capillary forces, bulk forcing, fluidization

Calculating yield stress of solid materials is an almost two century old problem for which many yield criteria have been proposed [1, 2]. Most of these criteria suggest existence of a conical failure surface in the principal stress space that describes yielding of ductile materials. The Rose failure surface, the von-Mises and Tresca envelopes are among those criteria. Although most of these theories have successfully predicted the behavior of solid materials under external shear forces, however, the existence of a satisfactory theory for discrete materials is under extreme debate [3].

Granular materials are discrete mesoscopic particles that are able to develop yield stress [4]. Study of the yield stress of granular materials is an important issue both because of its importance for investigation of the so-called jamming phase diagrams [5], and the material properties of the granulates and powders. During the last century, many devices, such as shear testers, have been developed to determine the shear strength of ductile materials, however, the influence of the gravity and the dependence of the output results to sample preparation techniques unables the shear testers from obtaining satisfactory results at very small loads. Hence, the shear strength has to be calculated using extrapolation [6]. Accordingly, due to the difficulties on the measurement of the yield stress of granular systems, a comprehensive knowledge on this problem is missing. This so, in particular, for wet granulates that are able to develop yield stress below random close packing (RCP) limit [7–9].

In this paper, we present a straightforward numerical method for direct measurement of the yield stress of loose and dense random assemblies of granular materials based on the von-Mises yield criterion. We apply the method to measure the yield stress of frictionless wet disks of different packing fraction ϕ, and capillary bridge energy ε. We believe that our model can be used as a standard numerical shear tester for a wide variety of discrete systems such as colloids and granulates.

To describe the method, let us recall some principles from solid mechanics. According to the stress-strain relation, any external force acting on an object can cause deformation. Such deformation can be either elastic, *i.e.* reversible, or plastic, *i.e.* irreversible. To describe these processes in a quantitative manner, a principal stress space is traditionally considered. The principal components, σ_1 and σ_2, of the stress tensor in $2D$ can be obtained from

$$\sigma_{1,2} = \frac{S_{xx}+S_{yy}}{2} \pm \sqrt{(\frac{S_{xx}-S_{yy}}{2})^2 + S_{xy}^2} \qquad (1)$$

where S_{xx} and S_{yy} are normal stresses and S_{xy} is the shear stress. The stress tensor can be separated into the compressional and deviatoric parts in which the later is related to the deformations caused by shearing. The von-Mises yield criterion states that the plastic deformation of materials occurs when the second invariant of the deviatoric stress tensor reaches a critical value, *i.e., yield stress*, σ_y, which can also be expressed as a function of the principal components of the stress tensor $\sigma_{1,2}$, as

$$\sigma_y^2 = \sigma_1^2 + \sigma_2^2 - \sigma_1\sigma_2 \qquad (2)$$

for the case of pure plane stress.

Fig. 1 shows a schematic $2D$ principal stress space, $\sigma_1 - \sigma_2$, where the yield surface illustrated as a brown-colored elliptical curve. Each point in this plane is related to a certain set of applied shear forces. Granular materials jam when the applied stress becomes smaller than the yield stress. Therefore, the golden area enclosed by the yield curve indicates the jammed region where the particles are dynamically arrested. When a system is unable to develop the yield stress, the golden area vanishes. For instance, for dry, frictionless spheres below the RCP limit, the golden area does not exist. From the computational point of view, a driving mechanism is needed to vary the position of the system in the principal stress space. By applying a constant shear rate, $\dot{\gamma}$, the so-called Lees-Ewards boundary conditions (LEbc), the

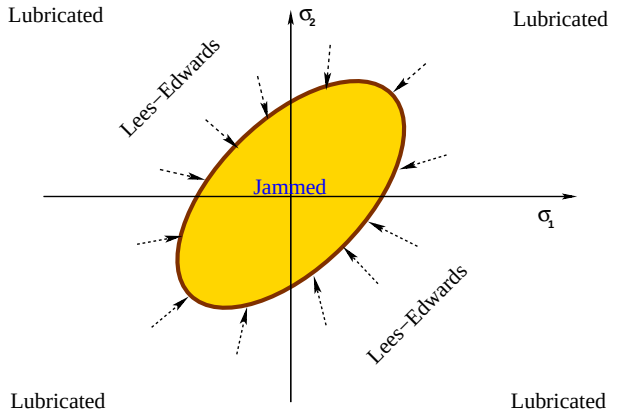

FIG. 1: Schematic of the von-Mises yield surface in a $2D$ principal stress space $\sigma_1 - \sigma_2$. The region inside the ellipsoidal curve indicates the jammed state for granular materials. The brown envelope is the yield curve and the outside area shows the lubricated regime. By enforcing the Lees-Edwards boundary conditions, one can move the state of the system towards and outwards the yield surface.

system is enforced to move through different positions in the principal stress space, hence, the applied shear rate, $\dot{\gamma}$, can be considered as a control parameter. However, since the LEbc enforce the system to flow with any arbitrary small shear rate, one can not probe the enclosed region, *i.e.,* the *jammed* state. Therefore, by applying the LEbc, the system will be brought to the outer region, *i.e.,* the *lubricated regime*, and, the jammed region will become the forbidden zone with the system being prevented from wandering in that area.

The basic idea for our method is that in LEbc by decreasing the shear rate, $\dot{\gamma}$, the system approaches to the yield surface, and at the vanishing limit of the shear rate, $\dot{\gamma} \to 0$, it becomes infinitesimally close to the yield surface. Providing that the system is able to develop the yield stress at the vanishing limit of the shear rate, $\dot{\gamma} \to 0$, all the components of the stress tensor should generate an offset. We believe that the offset of the stress tensor is associated with a point on the yielding envelope in the principal stress space. Therefore, knowing that point, enables one to calculate the yield stress according to the von-Mises yield criterion, *i.e.,* Eq. 2. In the proceeding, we utilize the proposed method for direct measurement of yield stress of wet granular material whose jamming phase diagram is not well-understood.

The stiffness of wet granular matter is originated from the cohesive forces exerted by the capillary bridges [7, 10–14]. While two adjacent granulates approach each other, no capillary bridge exists. A capillary bridge forms as soon as two neighboring granulates touch each other. Due to the surface tension of a capillary bridge, a cohesive force $F_{lb}(x)$ acts between two particles. This force decreases as a function of the separation, x, and switches off at a critical separation, S_c, where the capillary bridge ruptures. Accordingly, at any rupture event the energy equal to $\varepsilon = \int_0^{s_c} F_{lb}(x)\dot{dx}$ dissipates. The hysteretic nature of the capillary forces is the most important aspect of this attractive interaction [7, 13]. We engage a minimal capillary model proposed by Herminghaus in Ref. [7] in which the capillary force is constant as the distance between granulates changes. This model has been shown to be well-suited for numerical simulations of wet granular materials [8, 15, 16].

In the simulations, the minimal capillary force, F_c, is used as a force scale and the capillary bridge energy, ε, is the only free parameter determining the effect of capillary bridges. We use a 1:1 mixture of large and small disks of respective radii R_l and R_s with a ratio $R_l/R_s = 1.4$ to prevent the crystallization [17]. The RCP limit is reported to be $\phi_{\rm rcp} = 0.84$. Assuming a constant mass per area, ρ, the individual mass of disk i is $m_i = \pi\rho R_i^2$.

Mutual repulsion between the disks is modeled by a soft-core non-linear spring giving rise to a repulsive force

$$F_r(r_{ij}) = \begin{cases} C_{ij}(R_i + R_j - r_{ij})^{1/2} & \text{for } r_{ij} \le R_i + R_j \\ 0 & \text{else,} \end{cases} \tag{3a}$$

where r_{ij} is the Euclidean distance between the center of disk i and j. In the spirit of Hertz's contact law [19] we set

$$C_{ij} = C\left(\frac{R_i R_j}{R_i + R_j}\right)^{1/2} \tag{3b}$$

in order to account for different disk radii. The global parameter C controls the hardness of the disks.

Altogether, Newton's equation of motion for disk i reads

$$m_i \frac{d^2\mathbf{r}_i}{dt^2} = \sum_{j\in\mathcal{N}(i)} \mathbf{e}_{ij}\, f_{ij}(r_{ij}) \ , \tag{4}$$

where m_i and $\mathbf{r}_i$ are the mass and the position of disk i, respectively, $\mathcal{N}(i)$ is the set of neighbors j interacting with i, the unit vector $\mathbf{e}_{ij}$ points from the center of disk i to the center of disk j, and f_{ij} is the force exerted by disk i on disk j. The latter force comprises the soft-core repulsion (3), and whenever applicable also the attractive force, F_c, modeling capillary bridges. Eq. 4 is solved numerically using a fifth-order predictor-corrector Gear algorithm.

Throughout the remainder of this paper, we employ dimensionless rescaled quantities based on the capillary force, F_c, the mass density of the disks, ρ, and the average disk diameter D. Time, t, and mass, m, is hence measured in units $\tau \equiv \sqrt{\rho D^3/F_c}$, and $\mu \equiv \rho D^2$, respectively. Using these normalized quantities it is straightforward to normalize all physical quantities derived from mass, length and time, such as the local averages of disk velocities and the shear rate.

We found the implementation of LEbc challenging as the artifacts appear in the boundaries when the periodic coordinates of the particles are integrated. Instead, to prevent the cracks in the boundaries, the absolute coordinates of the particles must be integrated [20]. Finally, we note that all the collisions between particles are elastic except the capillary interactions.

The stress tensor, σ, can be given in the following form

$$\sigma = \sum_i (\mathbf{v}_i - \mathbf{U}(x)) \otimes (\mathbf{v}_i - \mathbf{U}(x)) + \sum_{i<j} \delta\mathbf{r}_{ij} \otimes \mathbf{F}_{ij} \quad (5)$$

where $\otimes$ is the tensor product, $\mathbf{v}_i$ is the velocity of the particle i, $\mathbf{U}(x) = \dot{\gamma}x$ is the local drift velocity at position x, $\delta\mathbf{r}_{ij}$ is the vector connecting centers of particle i and j, $\mathbf{F}_{ij}$ is the forces exerted by the particle i to particle j, and $\sum_{i<j}$ is the sum over the set of neighbors j interacting with particle i. Here, $S_{xy} = S_{yx}$ if all the interactions are central.

Fig. 2 depicts the components of the stress tensor subtracted by their corresponding offsets, as a function of the shear rate, $\dot{\gamma}$. In this plot, we demonstrate how the offsets of the stress tensor are extracted. The data are computed by averaging over a long period of time in the dynamic stationary state. The packing fraction has been taken $\phi = 0.8$, the capillary energy $\varepsilon = 0.01$, and the box length $L = 20$. The red(□) squares indicate the shear stress, S_{xy}, and the black (○) and blue (◇) points show the normal stresses, S_{xx} and S_{yy}, along x and y directions, respectively. The plot demonstrates a typical response of the system to the LEbc. As anticipated, all the components of the stress tensor develop offsets meaning that the jammed region in the principal stress space does exist. It is remarked that the components of the stress tensor decay exponentially. Fig. 2-inset shows the granular temperature, T_G, as a function of the shear rate. The granular temperature, T_G, decays very fast, almost exponentially, by decreasing the shear rate.

The next step is to define the dependence of the yield stress on the packing fraction, ϕ. Fig. 3 refers to this issue where the yield stress, σ_y, versus the packing fraction, ϕ, is shown. The upper limit of ϕ is the RCP limit $\phi_{rcp} = 0.84$ reported by *cf.* [17, 18]. For $\phi < 0.54$, as observed in *cf.* [9], particles condense into separate shear bands that move in opposite directions. Therefore, for $\phi < 0.54$, existence of a percolation cluster becomes history dependent and definition of the yield stress is ambiguous. Each point in the plot is calculated from an average over 20 different initial conditions. The black(○), red(□) and blue(◇) symbols refer to the capillary energy $\varepsilon = 0.01$, 0.05, and 0.1, respectively. It is observed that all the points diverge at the RCP limit. The solid lines in the plot show the best fits to data. The fitting functions is obtained to be

$$\sigma_y \sim (\frac{\phi}{\phi_{rcp} - \phi})^{2/3} \phi^2 \quad (6)$$

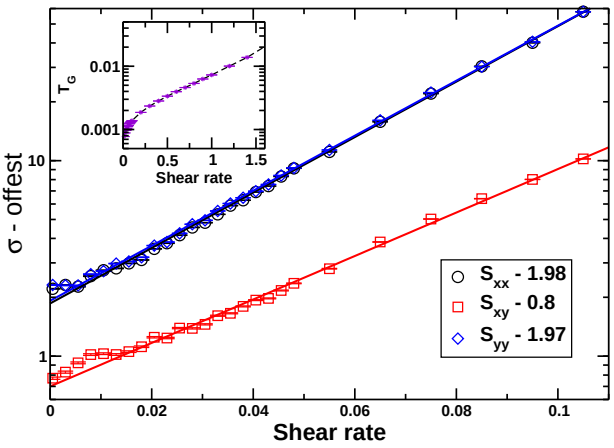

FIG. 2: Components of the stress tensor subtracted by their corresponding offsets as a function of the shear rate, $\dot{\gamma}$, for wet disks driven by the Lees-Edwards boundary conditions. The red(□), black (○), and blue (◇) points show S_{xy}, S_{xx}, and S_{yy} respectively. The components of the stress tensor decay exponentially by decreasing the shear rate $\dot{\gamma}$. The packing fraction has been taken $\phi = 0.8$, the capillary energy $\varepsilon = 0.01$, and the box length $L = 20$. Inset: The granular temperature versus the shear rate. The granular temperature decays also very fast by decreasing the shear rate. The dependency seems to be very close to the exponential decay.

where $1/(\phi_{rcp} - \phi)$ is the free volume for two disks to pass, and $\phi/(\phi_{rcp} - \phi)$ is the minimum number of disks that must be displaced in order to let two disks pass [9]. The yield stress shows strong dependence on the packing fraction, ϕ, close to the RCP limit, while it diverges at the $\phi_{rcp} = 0.84$. Furthermore, for a given packing fraction, ϕ, the yield stress increases upon increasing the capillary energy ε.

It is clear that the proportionality constant in Eq 6 is a function of the capillary energy ε. Varying the capillary energy for a fixed packing fraction, ϕ, reveals (*cf.* Fig.4) that this prefactor scales as $\varepsilon^{1/2}$. These dependencies of the yield stress, σ_y, to the packing fraction, ϕ, and the capillary energy, ε, leads to the following relation for the yield stress

$$\sigma_y \simeq B\varepsilon^{1/2} (\frac{\phi}{\phi_{rcp} - \phi})^{2/3} \phi^2 \quad (7)$$

in which the numerical prefactor $B = 9.1 \pm 1.1$. This dependence is demonstrated by a data collapse shown in Fig. 5 in which all the data from Fig. 3 and 4 collapse into almost the same value.

In conclusion, we provided a generic algorithm for direct measurement of the yield stress of discrete materials. To demonstrate the applicability of the algorithm, we successfully applied the method for the measurement of the yield stress of wet disks. Fig. 5 may be interpreted as a first jamming phase diagram of wet granular

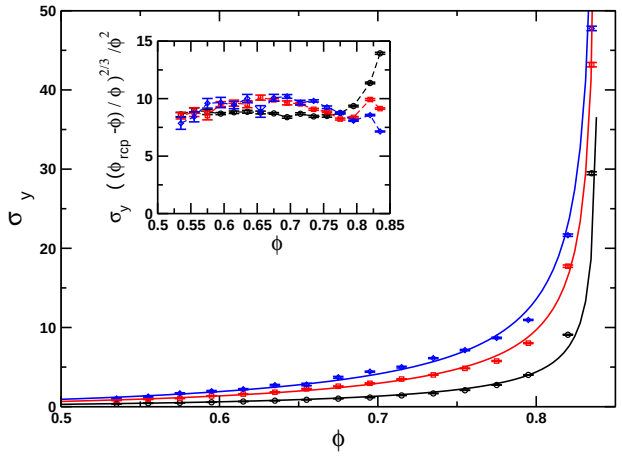

FIG. 3: Dependence of the yield stress, σ_y, to the packing fraction ϕ. The black(○), red(□) and blue(◇) points are obtained from averaging over 20 different simulations and correspond to three different capillary energy, $\varepsilon = 0.01$, 0.05, and 0.1, respectively. The solid lines show the best fit to the data based on Eq. 6. To emphasis this dependence, the inset shows that $\sigma_y((\phi_{rcp}-\phi)/\phi)^{2/3}/\phi^2$ takes almost constant values. All the curves diverge at the RCP limit. For a given packing fraction, ϕ, the yield stress increases upon increasing the capillary energy ε. The box length has been taken $L = 20$.

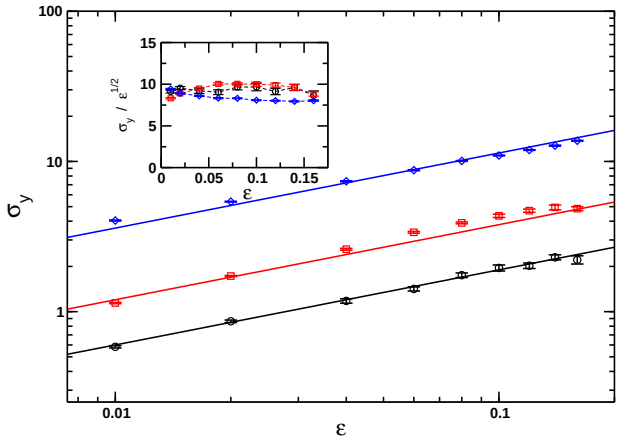

FIG. 4: Yield stress, σ_y, as a function of the capillary bridge energy, ε, for three different packing fractions $\phi = 0.6$, 0.7, and 0.8 depicted by the black(○), red(□), and blue(◇) points, respectively. Each point is an ensemble average of 20 different samples. The yield stress scales with the capillary energy as $\varepsilon^{1/2}$. To emphasis this dependence, the inset shows that $\sigma_y/\varepsilon^{1/2}$ which takes almost constant values. The system size has been taken $L = 20$.

materials which to our best knowledge has not yet been reported. We believe that this algorithm can be used for the measurement of the jamming phase diagram of a wide range of granular systems such as frictional or non-spherical particles. The method is also suites for the colloidal systems and wet foams.

We would like to thank M. Akbari-Moghanjoughi for his comments. This work is financially supported by the INSF Grant No. 90004064.

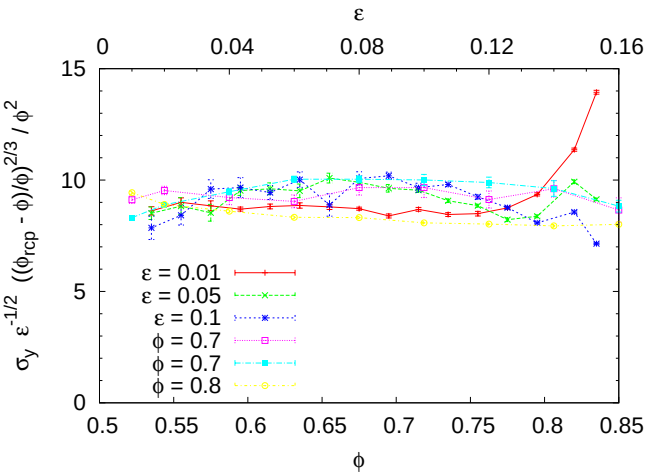

FIG. 5: All data of the yield stress, σ_y, that are also shown in Fig. 3 and 4. The data collapse indicates that the yield stress, σ_y, can be well described by Eq. 7 with a proportionally constant of the order 9.1. The parameters of the system are specified in the legend of the plot.

* Electronic address: sebrahi1@gwdg.de, habib.rahbari@gmail.com

[1] Y. Fung, Foundations of solid mechanics, Prentice Hall (1965).
[2] W. F. Chen, Studies in Applied Mechanics, vol. 2, Elsevier, **B**, 37 (1994).
[3] P. G. de Gennes, Rev. Mod. Phys. **71**, S374 (1999).
[4] M. E. Cates, J. P. Wittmer, J. P. Bouchaud, and P. Claudin, Phys. Rev. Lett. **81**, 1841 (1998).
[5] H.M. Jaeger and S.R. Nagel, Rev. Mod. Phys. **68**, 1259 (1996).
[6] T. Gröger, Ugur Tüzün, D. M. Heyes, Powder Technology, **133**, 203 (2003).
[7] S. Herminghaus, Adv. Phys. **54**, 221 (2005).
[8] S. H. Ebrahimnazhad Rahbari, J. Vollmer, S. Herminghaus and M. Brinkmann, Euro. Phys. Lett., **87**, 14002 (2009).
[9] S. H. Ebrahimnazhad Rahbari, J. Vollmer, S. Herminghaus, and M. Brinkmann, Phys. Rev. E., **82**, 61305 (2010).
[10] D.J. Hornbaker, R. Albert, I. Albert, A.L. Barabási, and P. Schiffer, Nature **387**, 765 (1997).
[11] Ch.D. Willet, M.J. Adams, S.A. Johnson, and J.P.K. Seville, Langmuir **16**, 9396 (2000).
[12] S. Nowak, A. Samadani, and A. Kudrolli, Nature Physics **1**, 50 (2005).
[13] N. Mitarai and F. Nori, Adv. Phys.**55**, 1 (2006).
[14] M. Scheel *et al.* Nat. Mat. **7**, 189 (2008); J. Phys.: Con-

dens. Matter **20**, 494236 (2008).
[15] A. Fingerle and S. Herminghaus, Phys. Rev. Lett.**97**, 078001 (2006).
[16] A. Fingerle and S. Herminghaus, Phys. Rev. E **77**, 011306 (2008).
[17] C.S. O'Hern, L.E. Silbert, A.J. Liu, and S.R. Nagel, Phys. Rev. E **68**, 011306 (2003).
[18] N. Xu, C.S. O'Hern, and L. Kondic, Phys. Rev. Lett. **94**, 016001 (2005); N. Xu, PhD thesis, Yale University (2005).
[19] T. Pöschel and T. Schwager, *Computational granular dynamics*, (Springer, New York, 2005).
[20] I. Goldhirsch, private communications.